INTERNATIONAL JOURNAL FOR NUMERICAL METHODS IN FLUIDS
Int. J. Numer. Meth. Fluids 2008; **58**:573–589
Published online 25 February 2008 in Wiley InterScience (www.interscience.wiley.com). DOI: 10.1002/fld.1784

Level-set based flamelet approach for simulating turbulent lifted jet flame

Sungmo Kang[1], Hoojoong Kim[1], Yongmo Kim[1,*,†,‡] and Kook-Young Ahn[2]

[1]*Department of Mechanical Engineering, Hanyang University, Seoul, Korea*
[2]*Korea Institute of Machinery & Materials, Daejeon 305-660, Korea*

SUMMARY

The present study focuses on numerically investigating the flame structure, flame liftoff, and stabilization in a lifted turbulent H_2/N_2 jet flame with a vitiated coflow. To realistically represent the turbulent partially premixed nature in the flow region between nozzle exit and flame base, the level-set approach coupled with the conserved scalar flamelet model has been applied. The unstructured-grid level-set approach has been developed to allow the geometric flexibility and computational efficiency for the solution of the physically and geometrically complex reacting flows. The pressure–velocity coupling is handled by the multiple pressure-correction method. The predicted flame pattern is in good conformity with the measured one. In terms of the liftoff height, the agreement between prediction and experiment is quite good. Even if there are noticeable deviations in a certain region, the predicted profiles for the overall flame structure agree reasonably well with the experimental data. These numerical results indicate that the present level-set-based flamelet approach in conjunction with the unstructured-grid finite-volume method is capable of realistically predicting the essential features and precise structure of the turbulent-lifted jet flame with computational efficiency. Copyright © 2008 John Wiley & Sons, Ltd.

Received 10 July 2007; Revised 15 January 2008; Accepted 17 January 2008

KEY WORDS: level-set approach; flamelet model; unstructured grid; flame stabilization; lifted flame; vitiated coflow

1. INTRODUCTION

The flame liftoff characteristic considerably influences the flame stabilization and pollutant formation in practical combustion devices and largely depends on flow configurations, fuel type, heat

*Correspondence to: Yongmo Kim, Department of Mechanical Engineering, Hanyang University, 17 Haengdang-Dong, Sungdong-Gu, Seoul 133-791, Korea.
†E-mail: ymkim@hanyang.ac.kr
‡Professor.

Contract/grant sponsor: Carbon Dioxide Reduction & Sequestration Research Center; contract/grant number: AE2-101-1-0-1

losses, mixing conditions, etc. The lifted partially premixed turbulent jet flames involve many fundamental mechanisms, which contain flame ignition, local extinction, re-ignition, and flame propagation. Since these physical phenomena are strongly coupled and highly nonlinear, explanations of the stabilization mechanism have been quite controversial. Theories for the flame stabilization mechanism may be divided into three categories including the premixed flame propagation theory [1], the flamelet quenching theory [2], and the large-scale eddy control mechanism [3]. According to the measurement [4] performed by Pitts, none of these theories could satisfactorily explain the stabilization mechanism of the partially premixed turbulent lifted flames.

In dealing with the non-premixed turbulent flames, the reliable and robust combustion models including the laminar flamelet concept [5] and the conditional moment closure [6] have been well developed. However, many combustion models for turbulent premixed or partially premixed flames were not quite successful for the design analysis of combustors due to their complexities and limitations. Hence, the *ad hoc* approach like the eddy dissipation model is quite often applied to the industrial design analysis. The more advanced models were suggested by Bray and Libby [7], Bradley *et al.* [8], Peters [5], and Zimont *et al.* [9]. For modeling turbulent flame propagation in partially premixed systems, Bradley *et al.* [8] proposed a strained premixed flamelet model in which combustion proceeds essentially as premixed turbulent flame propagation with the flammability limits imposed as a constraint, and mean heat release rate was evaluated by integrating over the probability density functions (PDFs) of both the reaction progress variable and mixture fraction. Later on, Bradley *et al.* [10] improved this model by allowing for premixed flame extinction at both positive and negative strain rates, and a Reynolds stress model and second-order closure for the temperature are used. Based on DNS results, Domingo and Vervisch [11] suggested the triple flame propagation mechanism to explain the stabilization of the partially premixed turbulent flames. Their numerical results clearly indicated that the triple flames are able to sustain strong interaction with vortices by adjusting their flame structure to a transient flowfield, thus being more robust than the pure diffusion flames. As another flamelet model for partially premixed situation, Chen *et al.* [12] proposed the level-set approach based on the two scalar fields, $G(x,t)$, which determines the location of the premixed flame front, and $Z(x,t)$, which express the state of mixing, to predict the liftoff heights for methane/air- and propane/air-lifted flames. This level-set approach combined with the conserved scalar flamelet model requires the formulations for premixed and non-premixed combustion. This approach is able to account for the triple-flame structure as a key element of the partially premixed situation. Based on the concept that the turbulent partially premixed flame propagation proceeds by an ensemble of laminar triple flamelets, the mean turbulent burning velocity is estimated in context with the PDF numerics. Their numerical results [12] indicate that the predicted liftoff heights agree reasonably well with the experimental data. However, no comparison has been made for the detailed flame structure. On the other hand, their level-set formulation discretized in the structured-grid system has severe limitations to apply to the real combustion systems, such as the geometrically complex gas turbine combustors.

In the present study, in order to realistically represent the turbulence–chemistry interaction in the partially premixed turbulent lifted jet flames, the level-set-based flamelet approach suggested by Chen *et al.* [12] has been adopted. In order to allow the geometric flexibility and computational efficiency for the solution of the physically and geometrically complex reacting flows, unlike the original level-set procedure [12] implemented in the structured-grid system, the present level-set-based flamelet procedure has been numerically formulated in conjunction with the unstructured-grid finite-volume method (FVM). This unstructured-grid level-set approach has been applied to numerically simulate the flame stabilization and combustion processes of the lifted turbulent H_2/N_2

DOI: 10.1002/fld

jet flame [13] with a vitiated coflow. Based on numerical results obtained in this study, a detailed comparison has been made in terms of the liftoff height and the detailed flame structure.

2. PHYSICAL AND NUMERICAL MODELS

The density-weighted Navier–Stokes equation, k–ε turbulent model equation, energy equation, and mean and variance of mixture fraction equations are employed to predict the turbulent reacting flows in cylindrical coordinate and represented as follows:

$$\frac{\partial}{\partial t}(\bar{\rho}\phi)+\frac{\partial}{\partial x_j}(\bar{\rho}\tilde{u}_j\phi)=\frac{\partial}{\partial x_j}\left(\Gamma_\phi\frac{\partial\phi}{\partial x_j}\right)+S_\phi \tag{1}$$

where ϕ includes the mean axial and radial velocity, mean enthalpy, turbulent kinetic energy and dissipation rate, mean and variance of mixture fraction, and Γ_ϕ and S_ϕ represent the diffusion coefficient and source term of its equation, respectively. The diffusion coefficients and source terms are well described in Reference [14].

2.1. *Level-set-based flamelet approach*

At the base of the lifted turbulent diffusion flame, fuel and oxidizer are partially premixed. The instantaneous surface of stoichiometric mixture separates lean and rich regions. When a flame propagates through the inhomogeneous fluctuating mixture of fuel and oxidizer, an instantaneous flame front separates burned and unburned gases. Thus, a formulation for both premixed and non-premixed combustion has to be used. In order to properly account for the turbulence–chemistry interaction in the partially premixed turbulent lifted jet flames, the present study has adopted the level-set-based flamelet approach suggested by Chen *et al.* [12]. In this approach, the flamelet model of non-premixed combustion is combined with the level-set approach for premixed combustion. The mixing of fuel and oxidizer in the turbulent flow field is described by transport equation of mean mixture fraction and its variance [5]. For the convenience of presentation, the important part of the level-set-based flamelet formulations proposed by Chen *et al.* [12] is described here.

In the level-set-based flamelet approach, the level-set approach [5, 15] based on the G-equation is employed to account for the premixed combustion process. The surface of the instantaneous premixed flame front $G(x,t)=G_0$ divides the flow field into regions of burned gas, $G(x,t)>G_0$, and unburned gas, $G(x,t)<G_0$. Since G is a non-reacting scalar, it avoids complications associated with counter-gradient diffusion and there is no need for a source term closure. The equation for the mean location of the turbulent flame front can be expressed as [5]

$$\frac{\partial(\bar{\rho}\tilde{G})}{\partial t}+\nabla\cdot(\bar{\rho}\tilde{v}\tilde{G})=\bar{\rho}s_{\mathrm{T},p}|\nabla\tilde{G}|-\bar{\rho}D_{\mathrm{t}}\tilde{\kappa}|\nabla\tilde{G}| \tag{2}$$

$$\tilde{\kappa}=\nabla\cdot\tilde{n}=\nabla\cdot\left(-\frac{\nabla\tilde{G}}{|\nabla\tilde{G}|}\right) \tag{3}$$

DOI: 10.1002/fld

where $\tilde{\kappa}$ is the curvature of the mean flame front, $\tilde{n}$ is a unit normal to the flame front, and D_t is the turbulent diffusivity. The equation for the variance of G can be expressed as [5]

$$\frac{\partial(\bar{\rho}\tilde{G}''^2)}{\partial t}+\nabla\cdot(\bar{\rho}\tilde{v}\tilde{G}''^2)=\nabla_{\|}\cdot(\bar{\rho}D_t\nabla_{\|}\tilde{G}''^2)+2\bar{\rho}D_t(\nabla\tilde{G})^2-c_s\bar{\rho}\frac{\tilde{\varepsilon}}{\tilde{k}}\tilde{G}''^2 \tag{4}$$

where $\nabla_{\|}$ denotes differentiation only tangential to the mean flame front.

To model the turbulent flame speed, $s_{T,p}$, of partially premixed flame in the mean location of the turbulent flame front, it is assumed that fuel and oxidizer are locally premixed such that the partially premixed flame propagates through a stratified and locally premixed mixture. According to Peters [5], the turbulent burning velocity s_T for the turbulent premixed flame can be determined from

$$\frac{s_T-s_L}{v'}=-\frac{a_4b_3^2}{2b_1}Da+\left[\left(\frac{a_4b_3^2}{2b_1}Da\right)^2+a_4b_3^2Da\right]^{1/2} \tag{5}$$

Here, s_L is the laminar flame speed, $Da=s_Ll/(v'l_F)$ is the Damköhler number, l and l_F are the integral length scale and the laminar flame thickness, v' is the turbulent intensity, and a_4, b_1 and b_3 are the model constants. The conditional turbulent flame speed, $s_T(Z)$, can be expressed in terms of a conditional turbulent Damköhler number, $Da(Z)$

$$s_T(Z)=s_L(Z)+v'F\{Da(Z)\} \tag{6}$$

Here, $F\{\}$ denotes the right-hand side term of Equation (5).

The mean turbulent burning velocity [12] of a partially premixed flame can be formulated by employing the presumed PDF approach

$$(\bar{\rho}s_{T,p})=\int_0^1\rho(Z)s_T(Z)P(Z)\,\mathrm{d}Z \tag{7}$$

where the PDF for mixture fraction, $P(Z)$, is presumed as the beta PDF. $s_T(Z)$ and $\rho(Z)$ are evaluated for the unburned mixture with the mixture fraction, Z.

In the partially turbulent premixed flame field, the diffusion flamelet structure is taken into account for two possible mixtures [12] that are either burning ($G>G_0$) or non-burning ($G<G_0$). For the burning flamelets, the mean mass fractions of the chemical species can be obtained by utilizing a flamelet library with the conditional scalar dissipation rate χ_{st} as a parameter. Thus, the mean mass fractions for the burned gas are computed by employing a presumed PDF approach:

$$\tilde{Y}_{i,b}(\tilde{Z},\tilde{Z}''^2,\tilde{\chi}_{st})=\int_0^1 Y_i(Z,\chi_{st})P(Z)\,\mathrm{d}Z \tag{8}$$

$Y_i(Z,\chi_{st})$ is obtained from a flamelet library and the stoichiometrically conditioned scalar dissipation rate, χ_{st}, of the flamelets is set to be equal to the mean stoichiometrically conditioned scalar dissipation rate, $\tilde{\chi}_{st}$, which can be calculated from

$$\tilde{\chi}_{st}=\frac{\tilde{\chi}f(Z_{st})}{\int_0^1 f(Z)P(Z)\,\mathrm{d}Z},\quad f(Z)=Z^2\ln Z \tag{9}$$

$$\tilde{\chi}=c_\chi\frac{\tilde{\varepsilon}}{\tilde{k}}\tilde{Z}''^2,\quad c_\chi=2.0 \tag{10}$$

DOI: 10.1002/fld

Here, a beta function PDF is also used for the presumed PDF for mixture fraction, $P(Z)$. In case of the unburned mixture, all mass fractions are zero except those of fuel and oxidizer. Thus, these mass fractions of the unburned mixture are linearly varied with the mixture fraction

$$\tilde{Y}_{\mathrm{F,u}} = Y_{\mathrm{F},1}\tilde{Z}, \quad \tilde{Y}_{\mathrm{Ox,u}} = Y_{\mathrm{Ox},0}(1-\tilde{Z}) \tag{11}$$

When the mixture exists within the turbulent flame brush, the averaged mass fractions are evaluated from the weighted sum

$$\tilde{Y}_i = p_{\mathrm{b}}\tilde{Y}_{i,b} + (1-p_{\mathrm{b}})\tilde{Y}_{i,u} \tag{12}$$

where p_{b} represents the probability of finding burned gas

$$p_{\mathrm{b}} = p_{\mathrm{b}}(G > G_0) = \int_{G=G_0}^{\infty} \frac{1}{\sqrt{2\pi\tilde{G}''^2}} \exp\left(-\frac{(G-\tilde{G})^2}{2\tilde{G}''^2}\right) \mathrm{d}G \tag{13}$$

Here, the PDF of G is assumed as a Gaussian distribution.

2.2. *Pressure-based unstructured-grid FVM*

To discretize the spatial domain in context with the unstructured-grid FVM, the cell-centered, collocated scheme is employed here because the control volume can be represented by the numerical grid itself and the coding structure including the imposition of boundary conditions can be further simplified. The cell types may be triangular and quadrilateral for 2-D problems, and tetrahedral, prism, pyramid, and hexahedral for 3-D problems. The cell type in each problem can be single or mixed. All transport variables are stored at cell centers. By integrating and also using the divergence theorem, the ϕ-transport equation can also be expressed in integral form as

$$\frac{\partial}{\partial t}\int_{\Omega} \rho\phi \,\mathrm{d}\Omega = \int_A \vec{F}\cdot\vec{n}\,\mathrm{d}A + \int_{\Omega} S_\phi \,\mathrm{d}\Omega \tag{14}$$

where Ω is the domain of interest, A the surrounding surface, and $\vec{n}$ the directional cosine of A in outward direction. The flux function $\vec{F}$ contains the inviscid and the diffusion flux vector

$$\vec{F} = -\rho\vec{u}\,\phi + \Gamma_\phi \nabla\phi \tag{15}$$

With the discretization of the spatial domain, the finite-volume formulation for the flux integral can be evaluated by the summation of the flux vector over each face f of a cell

$$\int_A \vec{F}\cdot\vec{n}\,\mathrm{d}A = \sum_{f=1}^{\mathrm{NB}} F_f A_f = \sum_{f=1}^{\mathrm{NB}} [-(\rho\vec{u}\cdot\vec{n})_f\phi_f + (\Gamma\nabla\phi\cdot\vec{n})_f]A_f = \sum_{f=1}^{\mathrm{NB}} (-J_f\phi_f + D_f) \tag{16}$$

where NB is the total surface number for cell P; similar to the number of neighbor cells which share a common face with cell P, A_f is the cell-face area, and J_f and D_f represent the mass flow rate and diffusive transport through the interfaces, respectively. As shown in Figure 1, at an interface f between cells P and E, the diffusion term can be approximated based on the second-order finite difference scheme for the tangent vectors and metric tensors in a curvilinear system. Here the primary diffusion is treated implicitly, whereas the cross-diffusion is handled explicitly. This formulation is quite robust due to its simplicity in the aspects of numerical implementation.

DOI: 10.1002/fld

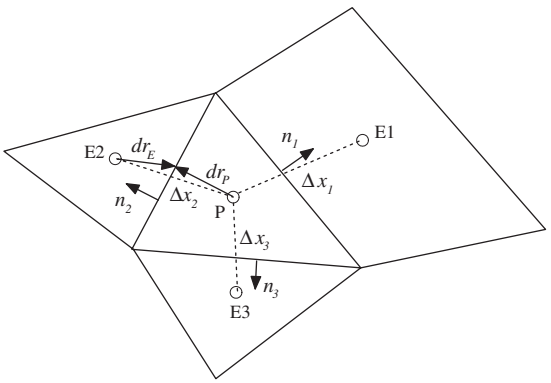

Figure 1. Illustration of the cell-centered control volumes for the 2-D arbitrary grid and all necessary geometric vectors for the reinitialization.

The second-order upwinding scheme is used for the convective flux terms. In this scheme, the face value is evaluated via the value at the upwind cell and a linear reconstruction procedure to achieve second-order accuracy. For the temporal integration, a general implicit-discretized time-marching scheme with a flux correction is employed for the system of linearized algebraic equations. In this integration procedure, various temporal schemes including the implicit Euler or Crank–Nicholson scheme can be constructed simply by changing the time-marching control parameter.

In this study, the pressure–velocity coupling in the chemically reacting flows is handled by the multiple pressure-correction method. Similar to the SIMPLE-family pressure-correction algorithm [16, 17], the pressure-correction equation is derived from the perturbed, equation of state, momentum, and continuity equations. In the present multi-corrector solution procedure [18], the entire corrector step is repeated for about four to six times to satisfy the continuity equation at the end of every time step. Then, the transport equations for scalars in mass fraction and temperature are solved sequentially. In order to avoid the well-known checkerboard flow fields, according to the concept of Rhie and Chow [19] developed for the structured-grid method, the pressure-damping term is introduced in context with the unstructured-grid procedure. The detailed formulations regarding the present pressure-based unstructured-grid FVM are described well in our previous work [14].

2.3. Reinitialization

The $\tilde{G}$-equation is only used to determine the mean flame position because the mean flame propagation speed, $s_{\mathrm{T},p}$, is only defined at the mean flame front. To avoid numerical difficulties, the scalar $\tilde{G}$ outside G_0 is calculated as a distance function. The reinitialization process [12] of the $\tilde{G}$-field has to be performed to satisfy $|\nabla\tilde{G}|=1$ outside the mean flame front. In general, in order to prevent the irregularities of the calculated level-set function, the reinitialization of the level-set function is needed during the entire computation. Since the zero-level set represents a moving flame front, it must not move during reinitialization. However, this zero-level set moves in actual computation and numerical error deviated from the zero-level set is introduced. In fact, the volume with the zero-level set shrinks and the volume is not conserved in the reinitialization process. In this study, the proper treatment proposed by Sussman and Fatemi [20] is employed to

DOI: 10.1002/fld

conserve the volume during the reinitialization process. The present reinitialization procedure is based on solving the following Hamilton–Jacobi equation:

$$\begin{aligned} \frac{\partial \phi}{\partial t} &= \operatorname{sign}(\phi_0)(1-|\nabla \phi|) \\ \phi(x,0) &= \phi_0(x) = \tilde{G}(x,t) - G_0 \end{aligned} \tag{17}$$

or in discretized form:

$$\phi^{n+1} = \phi^n - \Delta t \operatorname{sign}(\phi_0)(|\nabla \phi^n| - 1) \tag{18}$$

where the superscript n is the pseudo-time-marching number, Δt is a time step which is different from the flow time scale, and $\operatorname{sign}(\phi_0)$ is a sign function. This evolution equation has characteristics that originate at the flame surface and propagate the unitary gradient information from there into the surrounding field. Once the steady-state solution $\phi_\infty(x)$ is reached, then $\tilde{G}(x,t)$ is set equal to $\phi_\infty(x)$ for $\tilde{G} \neq G_0$ at that time step.

In context with unstructured-grid FVM, it is not easy to implement the higher-order finite difference approximation for an interface gradient. In the present study, the interface gradient is calculated by distance-weighted averaging of the cell-centered gradients of two cells sharing the interface. The present reinitialization procedure is summarized as follows:

1. Initialize $\phi(x, t=t_0) = \tilde{G}(x,t)$.
2. Search for zero-level set, i.e. cells near G_0 based on the sign-changing control surface.
3. Calculate the Heaviside function $H_{\Delta x}(\phi_0)$ and its derivative, and smoothed sign function $\operatorname{sign}(\phi_0)$:

$$H_{\Delta x} = \begin{cases} 1 & \text{if } \phi_0 > +\Delta x \\ 0 & \text{if } \phi_0 < -\Delta x \\ \dfrac{1}{2}\left[1 + \dfrac{\phi_0}{\Delta x} + \dfrac{1}{\pi}\sin\left(\dfrac{\pi\phi_0}{\Delta x}\right)\right] & \text{otherwise} \end{cases} \tag{19}$$

$$H'_{\Delta x} = \frac{1}{2}\left[1 + \frac{1}{\Delta x} + \frac{1}{\Delta x}\sin\left(\frac{\pi\phi_0}{\Delta x}\right)\right] \tag{20}$$

$$\operatorname{sign}_{\Delta x}(\phi_0) = 2(H_{\Delta x}(\phi_0) - 1/2) \tag{21}$$

   Here Δx is locally defined as the maximum value among the distances to the centroid of neighbor cells due to the spatially non-uniform grid as shown in Figure 1.
4. Start pseudo-time marching and repeat the following steps until the convergence criteria is satisfied. First begin with the calculation of interface gradient:

$$\overline{\nabla \phi_f} = (1-\alpha)\nabla \phi_P + \alpha \nabla \phi_E, \quad \alpha = \frac{dr_P}{dr_P + dr_E} \tag{22}$$

DOI: 10.1002/fld

5. Based on the upwinding scheme, $|\nabla\phi|$ is discretized:

$$\frac{\partial\phi}{\partial x_i} = \min\left(\text{sign}(\vec{n_i})_f \left.\frac{\partial\phi}{\partial x_i}\right|_f, 0.0\right) \quad \text{for } \phi_0>0 \quad (i=1,2,3;\ f=1,\ldots,\text{NB})$$
$$\frac{\partial\phi}{\partial x_i} = \max\left(\text{sign}(\vec{n_i})_f \left.\frac{\partial\phi}{\partial x_i}\right|_f, 0.0\right) \quad \text{for } \phi_0<0 \tag{23}$$

Here $\vec{n_i}$ is the direction cosine of control surface f in outward direction and NB is the total surface number of a cell.

6. Let $\tilde{\phi}^{n+1} = \phi^n - \Delta t\,\text{sign}(\phi_0)(|\nabla\phi^n|-1)$.

Here Δt is globally defined based on the minimum distance between centroids of two cells, $\Delta x_{\min}$ and a CFL condition of 0.1 such as $\Delta t = 0.1\Delta x_{\min}$.

7. Impose the volume conservation [20]:

$$\phi^{n+1} = \tilde{\phi}^{n+1} + \Delta t\,\lambda H'_{\Delta x}(\phi_0)|\nabla\phi_0| \tag{24}$$

where

$$\lambda = \frac{-\int_\Omega H'_{\Delta x}(\phi_0)(\tilde{\phi}^{n+1}-\phi_0)/\Delta t}{\int_\Omega [H'_{\Delta x}(\phi_0)]^2|\nabla\phi_0|} \tag{25}$$

3. RESULTS AND DISCUSSIONS

In order to validate the present unstructured-grid level-set-based flamelet approach as well as systematically investigate the detailed flame structure and stabilization mechanism in the turbulent lifted jet flames, the turbulent lifted H_2/N_2 jet flame [13] with a coflow of lean H_2/air hot-combustion gases has been chosen as a validation case.

Cabra *et al.* [13] experimentally and numerically investigated a lifted turbulent H_2/N_2 jet flame in a coflow of lean H_2/air hot-combustion gases. The experimental condition is given in Table I. Figure 2 shows the schematics of experimental combustor which consists of a central H_2/N_2 turbulent jet with a coaxial flow of hot-combustion products from a lean premixed H_2/air flame. The central jet exit diameter and an outer diameter are 4.57 and 210 mm, respectively. This vitiated coflow burner has the advantage of representing both liftoff and autoignition in a rather simple flow configuration and nearly stationary flame field. However, it is necessary to note that lifted flames issuing in vitiated coflow are different from those stabilized flames in cold slow-velocity coflow or stagnant air. The detailed scalar measurements [13] including temperature and concentrations of the major species, OH and NO, are available for a lifted turbulent nitrogen–diluted hydrogen jet flame ($Re=23\,600$) with a lean H_2/air vitiated coflow ($\phi=0.25, T=1045\,\text{K}$). Centerline measurements were taken from $z/d=1$–34 downstream of the nozzle exit. Radial profiles were obtained at seven axial stations. The stoichiometric mixture fraction for the present fuel composition is $Z_{\text{st}}=0.474$. The chemical kinetics of hydrogen is based on Mueller mechanism involving 9 species and 21 elementary reactions [21].

In the solution procedure of the present level-set-based flamelet approach, the non-reacting mixing field was first calculated for the given boundary condition. Then, the mixture was ignited

DOI: 10.1002/fld

at a downstream location by initialization of the G-field. The computation continues until the propagated flame front reached the flame base stabilized at a stationary lifted flame field. Near the

Table I. Boundary conditions for the lifted turbulent H_2/N_2 jet flame.

Central jet		*Coflow*	
Q_{H_2} (slm)	25	Q_{H_2} (slm)	225
Q_{N_2} (slm)	75	Q_{AIR} (slm)	2100
T_{JET} (K)	305	T_{COFLOW} (K)	1045
V_{JET} (m/s)	107	V_{COFLOW} (m/s)	3.5
Re_{JET}	23600	Re_{COFLOW}	18600
d_{JET} (mm)	4.57	D_{COFLOW} (mm)	210
X_{H_2}	0.2537	ϕ	0.25
X_{N_2}	0.7427	X_{O_2}	0.1474
		X_{H_2O}	0.0989
		X_{N_2}	0.7534

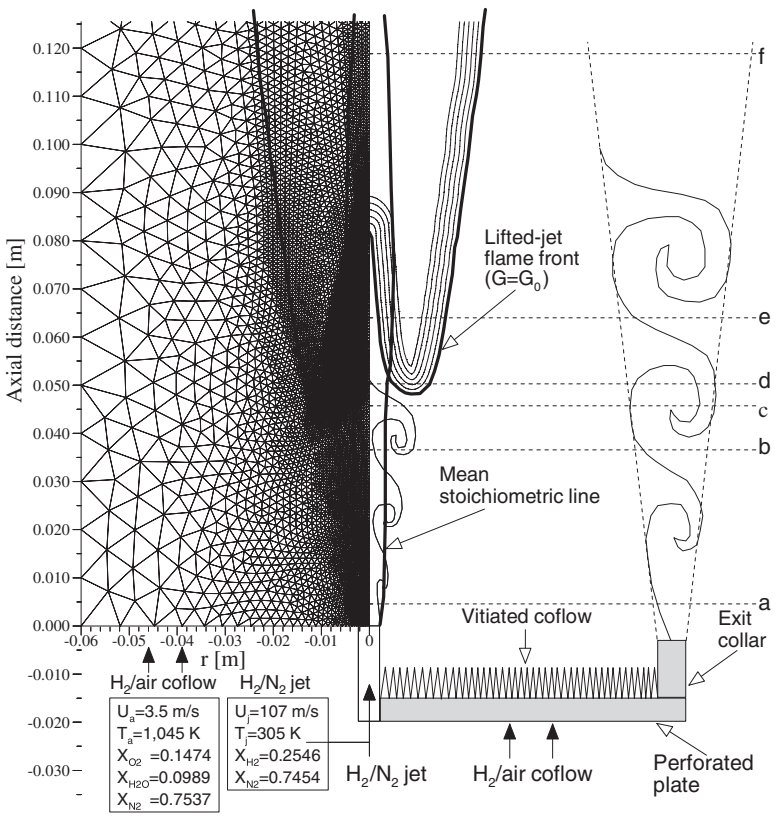

Figure 2. Schematic diagram and triangular grid for the lifted turbulent H_2/N_2 jet flame in a vitiated coflow at $Re = 23600$ ($d = 4.57$ mm, $U_j = 107$ m/s): npoin = 6871, ncell = 13289, nface = 19708, nbfac = 451.

DOI: 10.1002/fld

flame base, the net convective flux of G is balanced with the production of G due to the turbulent flame propagation and stabilization of the lifted flame is accomplished.

Figure 3 shows the predicted mean field of scalar G and mixture fraction near stabilization region for the coarse (7556 cells) and fine (13 289 cells) grid arrangement. Compared with the coarse grid, the fine grid yields much smoother contour lines of scalar G. In terms of the local profiles of species mass fraction and mixture fraction, the fine-grid results have slightly better conformity with measurements especially near the flame front. Thus, all computational results obtained in this study are based on 13 289 cells with the adaptive refinement at the high-gradient regions. In this predicted flame field shown in Figure 3, the flame base is stabilized at the location much leaner than the stoichiometric condition ($Z_{st}=0.474$). This stabilization characteristic of the lifted flames with the hot vitiated coflow is quite different from that of the turbulent lifted flames with cold slow-velocity coflow or stagnant air, which are stabilized at around the nearly stoichiometric flame base. It is speculated that this lifted jet flame with a vitiated coflow is characterized by the propagation of a turbulent partially premixed flame and the autoignition through the downstream mixing process of the vitiated coflow and the central H_2/N_2 jet.

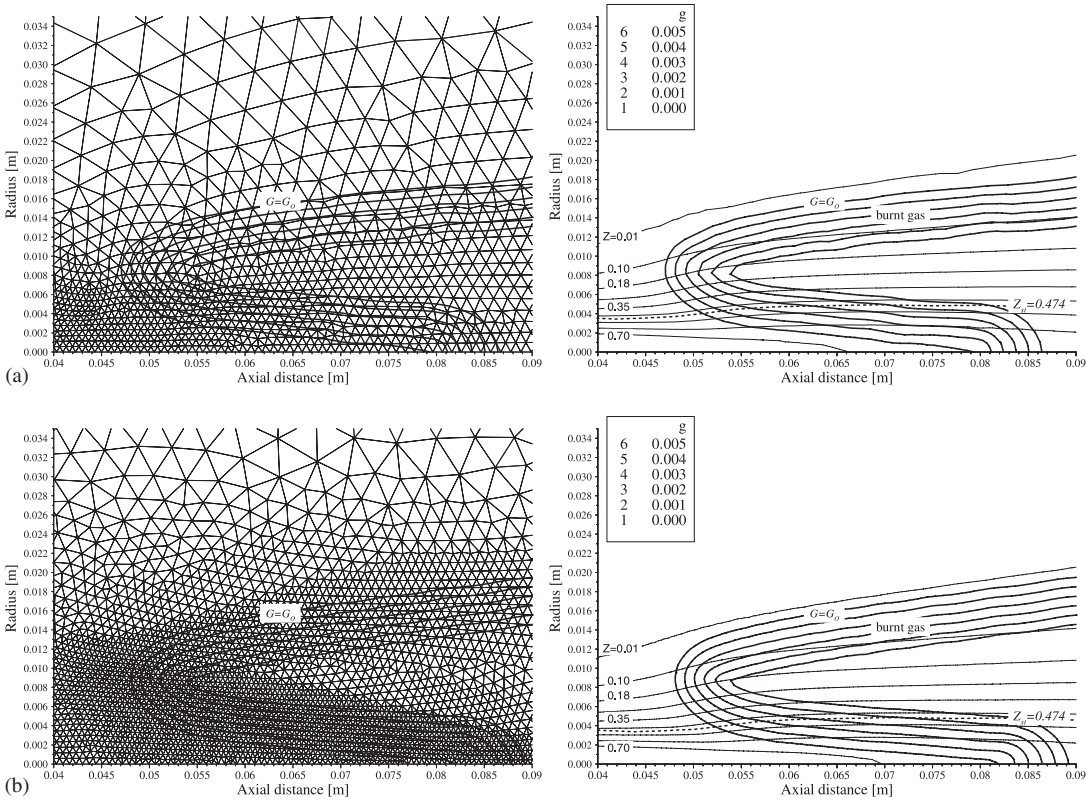

Figure 3. Predicted contours of mean scalar G and mixture fraction near the stabilization region for two grid arrangements: (a) coarse grid (ncell = 7556) and (b) fine grid (ncell = 13 289).

DOI: 10.1002/fld

Figure 4 shows the predicted contours of mean temperature and OH mass fraction in the lifted turbulent H_2/N_2 jet flame by utilizing the Mueller mechanism. The predicted flame pattern is in good conformity with the measured one [13]. The predicted liftoff heights are defined as the distance between nozzle exit and the lowest axial location of G_0. The liftoff heights predicted by the level-set approach favorably agree with the experimental data. In terms of the liftoff height, the agreement between prediction ($x/d = 10.53$) and experiment ($x/d = 10$) is quite good.

For comparison with measurement, Figures 5–7 present the centerline and radial profiles of mean temperature, mixture fraction, variance of mixture fraction, and O_2 mass fraction at six axial stations of $x/d = 1.0$, 8.0, 10.0, 11.0, 14.0, and 26.0, respectively. In terms of temperature and mixture fraction, the overall agreement between prediction and measurement is obtained. However, the variance of mixture fraction and the O_2 mass fraction is substantially underestimated at the downstream region of the flame base.

The significant underestimation of the mixture fraction fluctuations could be mainly attributed to the defect of the flamelet model, which is incapable of simulating the thickened turbulent flame regime generated by the turbulent eddies smaller than the reaction thickness, observed at around

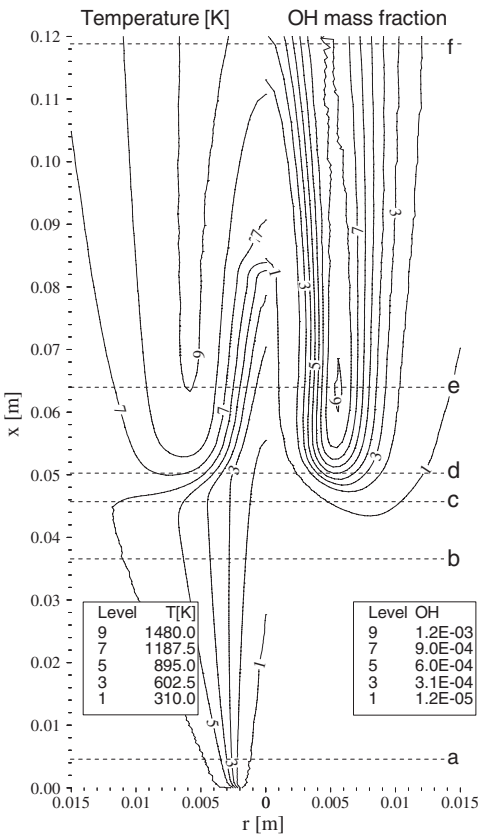

Figure 4. Predicted contours of mean temperature (K) and OH mass fraction in a lifted turbulent H_2/N_2 jet flame ($d = 4.57$ mm).

DOI: 10.1002/fld

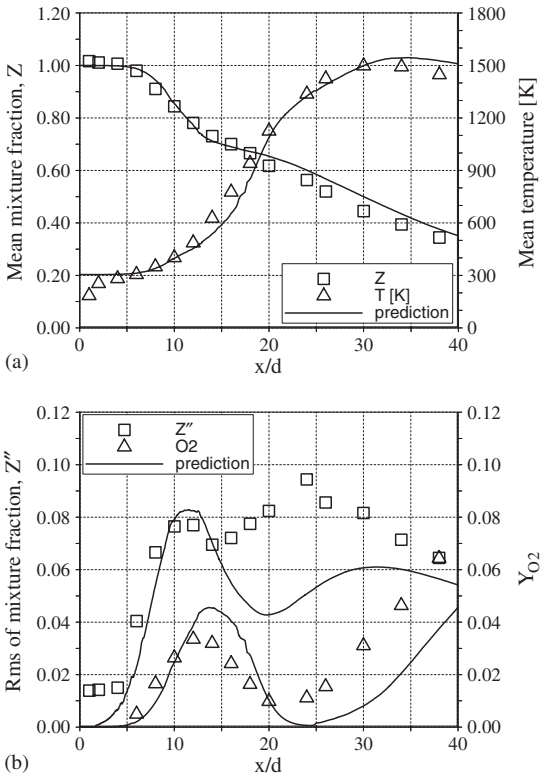

Figure 5. Centerline profiles of mean mixture fraction, temperature, rms of mixture fraction, and oxygen mass fraction. (a) Mean mixture fraction and temperature, (b) rms of mixture fraction and O_2 mass fraction. Symbols: experimental measurements [13]; line: prediction.

the flame base ($x/d=11$) in the experiment. This underestimation of mixture fraction fluctuations is also partly responsible for the defect of turbulent k–ε model and the uncertainty of inlet boundary condition for the variance of mixture fraction. The underestimated mixture fraction fluctuation is tied with the underpredicted scalar dissipation rate, which directly leads to the underestimation of the non-equilibrium effects, O_2 leakage, and O_2 penetration.

As shown in Figure 5, in the centerline distribution of O_2 mass fraction in the proximity of the flame base, the peak value of O_2 mass fraction is placed at $x/d=12$. In the downstream of the flame base, the oxygen entrained from the coflow oxidizer is continuously consumed and the O_2 mass fraction is correspondingly decreased up to the downstream region. In the far downstream region where fuel is completely consumed, the O_2 mass fraction gradually increases through the entrainment and turbulent mixing processes. In the downstream region of the flame base, the O_2 mass fraction underestimated. However, the predicted location ($x/d=12$) of peak O_2 mass fraction agrees well with the measured one. These numerical results suggest that the location of peak O_2 mass fraction is directly linked with the flame lifted height.

Figures 6 and 7 show the radial profiles of mixture fraction, temperature, and O_2 mass fraction. Even if there are noticeable deviations from measurement, in the overall flame structure, the

DOI: 10.1002/fld

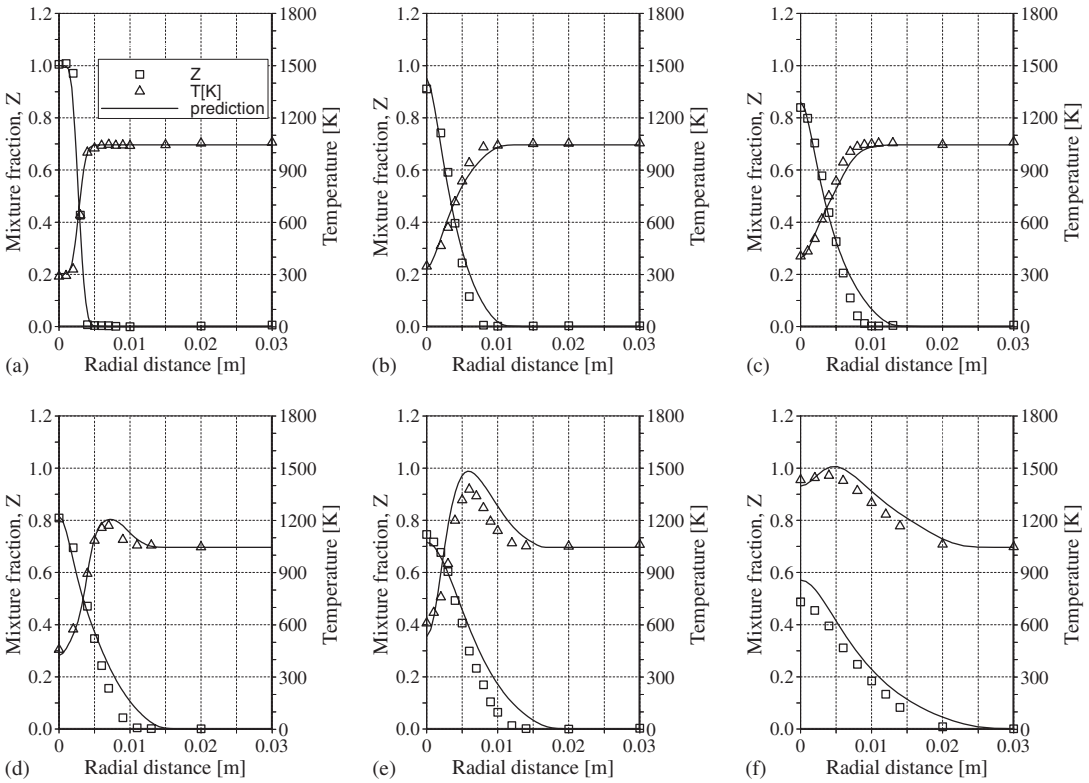

Figure 6. Radial profiles of mean mixture fraction and temperature. Symbols: experimental measurements [13]; line: prediction. (a) $x/d=1.0$; (b) $x/d=8.0$; (c) $x/d=10.0$; (d) $x/d=11.0$; (e) $x/d=14.0$; and (f) $x/d=26.0$.

predicted profiles agree reasonably well with the experimental data. Numerical results indicate that the present approach realistically simulates the essential features of the lifted turbulent H_2/N_2 jet flame with a vitiated coflow.

Figures 8 and 9 present the centerline profiles of H_2, H_2O, and OH, as well as their radial profiles at six axial stations. In comparison with measurement, the predicted mass fraction for H_2, H_2O, and OH have overall agreement with the experimental data. However, the mass fraction of H_2 and H_2O is overestimated at the downstream region of the flame base. Compared to measurements, the formation of OH radicals and location of centerline peak OH mass fraction occur at the slightly further downstream region. These deviations with measurements are in line with the underestimation of mixture fraction fluctuations mentioned above.

4. CONCLUSION

In order to validate the present unstructured-grid level-set-based flamelet approach as well as systematically investigate the detailed flame structure and stabilization mechanism in the turbulent

DOI: 10.1002/fld

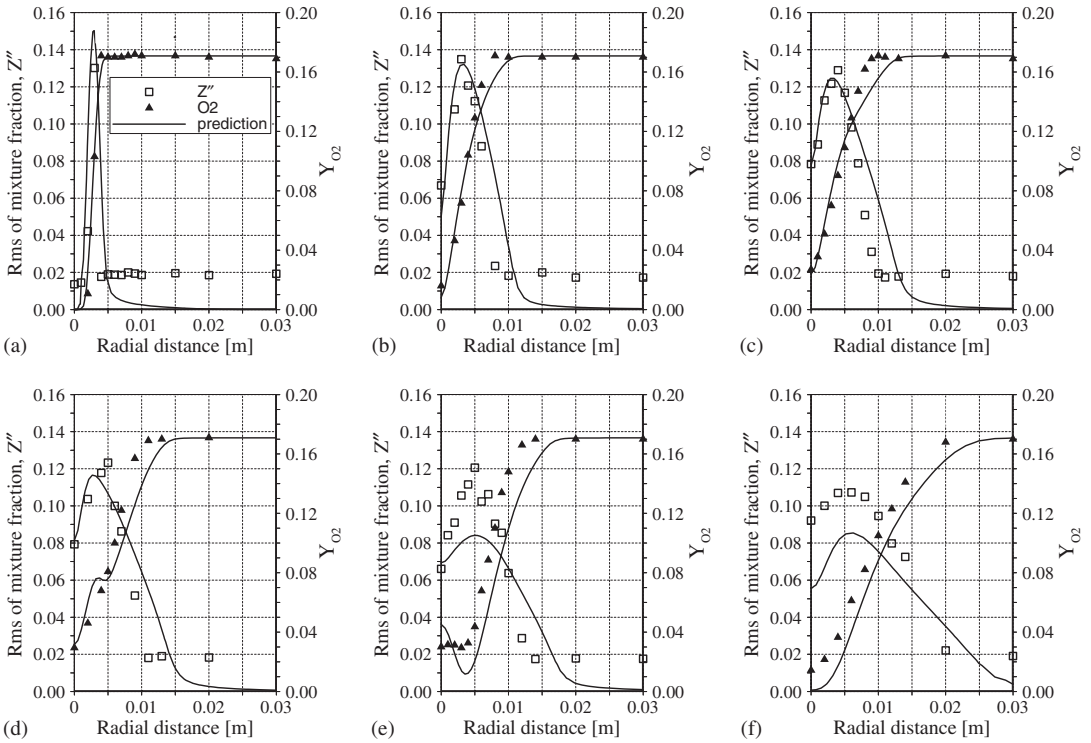

Figure 7. Radial profiles of rms of mixture fraction and O_2 mass fraction. Symbols: experimental measurements [13]; line: prediction. (a) $x/d = 1.0$; (b) $x/d = 8.0$; (c) $x/d = 10.0$; (d) $x/d = 11.0$; (e) $x/d = 14.0$; and (f) $x/d = 26.0$.

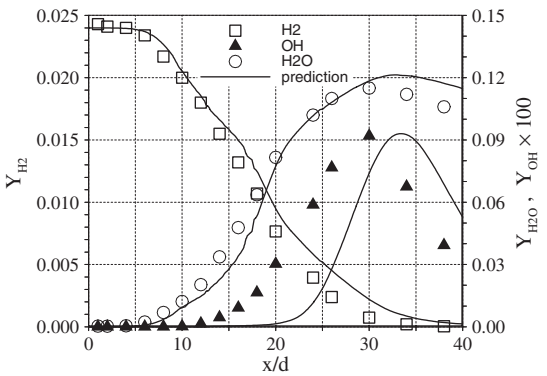

Figure 8. Centerline profiles of mean mass fractions of H_2, H_2O, and OH. Symbols: experimental measurements [13]; line: prediction.

lifted jet flames, the turbulent lifted H_2/N_2 jet flame with a vitiated coflow has been chosen as a validation case. Numerical results indicate that the present level-set-based flamelet approach in

DOI: 10.1002/fld

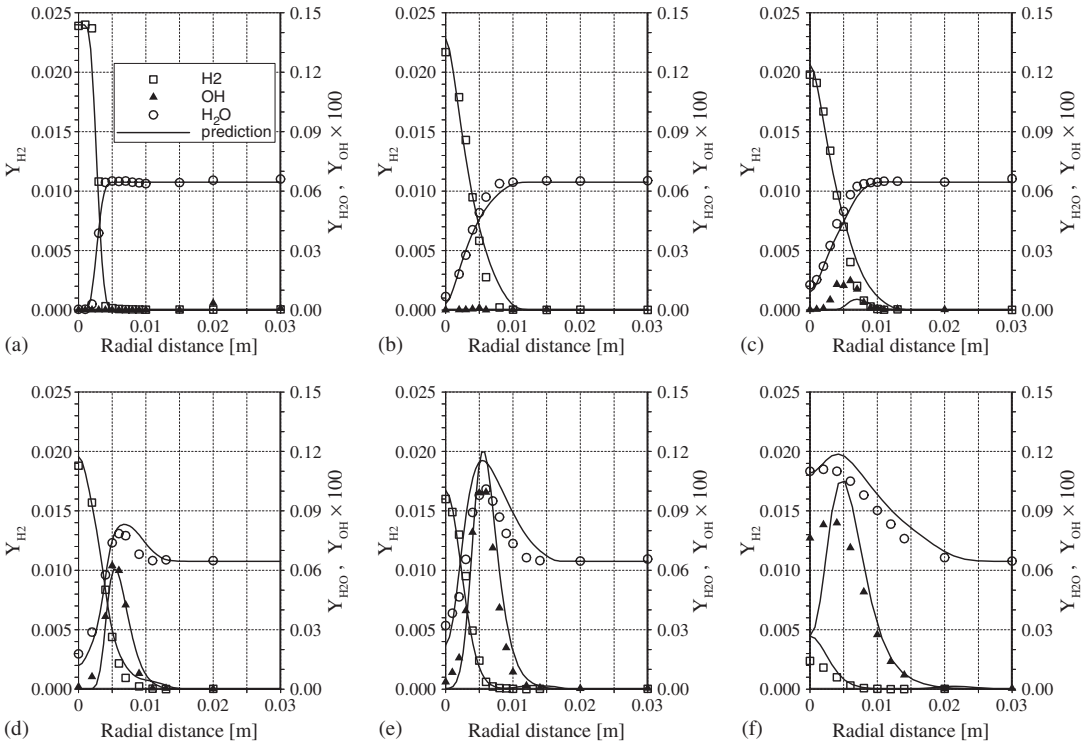

Figure 9. Radial profiles of mean mass fractions of H_2, H_2O, and OH. Symbols: experimental measurements [13]; line: prediction. (a) $x/d=1.0$; (b) $x/d=8.0$; (c) $x/d=10.0$; (d) $x/d=11.0$; (e) $x/d=14.0$; and (f) $x/d=26.0$.

conjunction with the unstructured-grid FVM has the capability to realistically predicting the essential features and precise structure of the turbulent lifted jet flame with computational efficiency.

The predicted flame pattern represented by the OH distribution is in good conformity with the measured one. The liftoff heights predicted by the level-set approach favorably agree with the experimental data. In terms of the liftoff height, the agreement between prediction ($x/d=10.53$) and experiment ($x/d=10$) is quite good. The flame base is stabilized at the location much leaner than the stoichiometric condition ($Z_{st}=0.474$). This stabilization characteristic of the lifted flames with the hot vitiated coflow is quite different from that of the turbulent lifted flames with cold slow-velocity coflow or stagnant air, which are stabilized at around the nearly stoichiometric flame base.

In terms of temperature and mixture fraction, the overall agreement between prediction and measurement is reasonably good. However, the variance of mixture fraction and the O_2 mass fraction is substantially underestimated at the downstream region of the flame base. The significant underestimation of the mixture fraction fluctuations could be mainly attributed to the defect of the flamelet model, which is incapable of simulating the thickened turbulent flame regime generated by the turbulent eddies smaller than the reaction thickness observed at around the flame base ($x/d=11$) in the experiment. This underestimation of mixture fraction fluctuations is also partly

DOI: 10.1002/fld

responsible for the defect of turbulent k–ε model and the uncertainty of inlet boundary condition for the variance of mixture fraction.

NOMENCLATURE

Da	Damköhler number
G	non-reacting scalar or distance function
l_{F}	laminar flame thickness
P	probability density function
p	static pressure
p_{b}	burning probability
t	time
T	flow temperature
s_{L}	laminar burning velocity
s_{T}	turbulent burning velocity
u_i	ith Cartesian velocity component
v	fluctuation velocity
x_i	physical coordinate
Y_i	ith species mass fraction
Z	mixture fraction
χ	scalar dissipation rate
$\tilde{\kappa}$	curvature of mean flame front
ρ	fluid density
$\phi_{0,1}$	values in oxidizer and fuel stream, respectively
$\phi_{\mathrm{b},u}$	values in burnt and unburnt mixtures, respectively
$\bar{\phi}$	Reynolds-averaged (density-unweighted) properties
$\tilde{\phi}$	Favre-averaged (density-weighted) properties

ACKNOWLEDGEMENTS

This research was supported by Grant AE2-101-1-0-1 from the Carbon Dioxide Reduction & Sequestration Research Center, one of the 21st Century Frontier Programs funded by the Ministry of Science and Technology of the Korean Government.

REFERENCES

1. Vanquickenborne L, Van Tiggelen A. The stabilization mechanism of lifted diffusion flames. *Combustion and Flame* 1966; **10**:59–69.
2. Peters N, Williams FA. Lift-off characteristics of turbulent jet diffusion flames. *AIAA Journal* 1983; **21**(3):423–429.
3. Broadwell JE, Dahm WJA, Mungal MG. Blowout of turbulent diffusion flames. *Proceedings of the 20th Symposium* (*International*) *on Combustion*. The Combustion Institute: Pittsburgh, PA, 1984; 303–310.
4. Pitts WM. Assessment of theories for the behavior and blowout of lifted turbulent jet diffusion flames. *Proceedings of the 22nd Symposium* (*International*) *on Combustion*. The Combustion Institute: Pittsburgh, PA, 1988; 809–816.
5. Peters N. *Turbulent Combustion*. Cambridge University Press: Cambridge, 2000.
6. Klimenko AY, Bilger RW. Conditional moment closure for turbulent combustion. *Progress in Energy and Combustion Science* 1999; **25**:595–687.
7. Bray KNC, Libby PA. *Turbulent Reacting Flows*. Academic Press: London, San Diego, New York, 1994; 309–374.

DOI: 10.1002/fld

8. Bradley D, Gaskell PH, Lau AKC. A mixedness-reactedness flamelet model for turbulent diffusion flames. *Proceedings of the 23rd Symposium* (*International*) *on Combustion.* The Combustion Institute: Pittsburgh, PA, 1990; 685–692.
9. Zimont VL, Biagioli F, Syed K. Modelling turbulent premixed combustion in the intermediate steady propagation regime. *Progress in Computational Fluid Dynamics* 2001; **1**(1/2/3):14–28.
10. Bradley D, Gaskell PH, Gu XJ. The mathematical modeling of liftoff and blowoff of turbulent non-premixed methane jet flames at high strain rates. *Proceedings of the 27th Symposium* (*International*) *on Combustion.* The Combustion Institute: Pittsburgh, PA, 1998; 1199–1206.
11. Domingo P, Vervisch L. Triple flames and partially premixed combustion in autoignition of non-premixed turbulent mixtures. *Proceedings of the 26th Symposium* (*International*) *on Combustion.* The Combustion Institute: Pittsburgh, PA, 1996; 233–240.
12. Chen M, Herrmann MG, Peters N. Flamelet modeling of lifted turbulent methane/air and propane/air jet diffusion flames. *Proceedings of the 28th Symposium* (*International*) *on Combustion*. The Combustion Institute: Pittsburgh, PA, 2000; 167–174.
13. Cabra R, Myhrvold T, Chen JY, Dibble RW, Karpetis AN, Barlow RS. Simultaneous laser Raman–Rayleigh-LIF measurements and numerical modeling results of a lifted turbulent H_2/N_2 jet flame in a vitiated coflow. *Proceedings of the Combustion Institute* 2002; **29**:1881–1888.
14. Kang S, Kim Y. Parallel unstructured-grid finite-volume method for turbulent nonpremixed flames using the flamelet model. *Numerical Heat Transfer B* 2003; **43**:525–547.
15. Williams FA. *Combustion Theory*. Benjamin/Cummins: Menlo Park, CA, 1985.
16. Patankar SV, Spalding DB. A calculation procedure for heat, mass and momentum transfer in three-dimensional parabolic flows. *International Journal of Heat and Mass Transfer* 1972; **15**:1787.
17. Van Doormaal JP, Raithby GD. Enhancements of the SIMPLE method for predicting incompressible flows. *Numerical Heat Transfer* 1984; **7**:147–163.
18. Kim YM, Chen CP, Ziebarth JP, Chen YS. Prediction of fast transient spray-combusting flows. *Numerical Heat Transfer A* 1994; **25**:21–42.
19. Rhie CM, Chow WL. Numerical study of the turbulent flow past an airfoil with trailing edge separation. *AIAA Journal* 1983; **21**(11):1525–1532.
20. Sussman M, Fatemi E. Level set redistancing algorithm. *SIAM Journal on Scientific Computing* 1999; **20**(4): 1165–1191.
21. Mueller MA, Kim TJ, Yetter RA, Dryer FL. Flow reactor studies and kinetic modeling of the H_2/O_2 reaction. *International Journal of Chemical Kinetics* 1999; **31**:113–125.

DOI: 10.1002/fld